Proceedings of the
Annual Stability Conference
Structural Stability Research Council
San Antonio, Texas, March 19-22, 2024

On the definition of geometrical imperfections in the F.E. modelling of CHS in compression

Mariana Echeverri[1], Pablo Rico[2], Liya Li[3], Carlos Graciano[4], Nicolas Boissonnade[5]

Abstract

This paper investigates the local buckling behavior of steel Circular Hollow Sections (CHS). Design recommendations for CHS are known to be somewhat conservative and sometimes inappropriate, namely with respect to section classification. CHS sections also provide a peculiar response to local buckling, being quite sensitive to initial geometrical imperfections (both with respect to their shape and amplitude), as a result of a shell-like response.

This paper reports numerical investigations towards a better characterization of initial imperfections in the response of CHS sections under compression. The results of non-linear shell F.E. sensitivity studies on geometrical imperfections are provided, comparing different shapes and amplitudes to literature results. Typically, the introduction of initial imperfections has relied on the first eigenmode; however, the local buckling response can vary significantly compared to experimental stub column tests in some cases, especially for slender sections. Finally, the paper concludes with practical modeling recommendations for more accurate representations of CHS section behavior under compression.

1. Introduction

The structural response of Circular Hollow Sections (CHS) is dominated by a shell-like response, contrary to Square and Rectangular Hollow Sections in which the behavior is plate-like. This difference results in CHS exhibiting structural performances that are highly dependent on initial imperfections. As classical references explain (Petersen, 2012, 2020; Rotter, 2023; S. Timoshenko, 1959; Ziemian, 2010), this peculiarity arises from the presence of nonzero third-order terms in the polynomial expansion of the total potential energy, as opposed to plates or columns where this term is zero (Bažant & Cedolin, 1991). Tests have demonstrated quite a number of different post-buckling shapes for shells under compression, including inward and outward buckling wave patterns, a "diamond shape" (sometimes also denoted as the Yoshimura pattern (Bažant & Cedolin, 1991; ESDEP, 2018)), or a so-called "elephant foot failure mode", see Fig. 1.

[1] MSc student, Universidad Nacional de Colombia, <mecheverrilo@unal.edu.co>
[2] PhD student, Laval University, <pablo.rico.1@ulaval.ca>
[3] Professor, Sherbrooke University, <liya.li@usherbrooke.ca>
[4] Professor, Universidad Nacional de Colombia, <cagracianog@unal.edu.co >
[5] Professor, Laval University,<nicolas.boissonnade@gci.ulaval.ca >

Figure 1: CHS failure modes. (a) Elephant foot failure (b) Diamond shape pattern (Guo et al., 2016).

Experimental series also indicate a rather non-uniform behavior depending on the slenderness of the section (e.g., diameter-to-thickness D / t ratio).

Through various experimental tests, notable disparities were noted between the predicted theoretical critical loads and the actual test loads, with failure loads sometimes as low as 10% of the theoretical critical load. Empirical knockdown factors were subsequently introduced in an attempt to design such types of sections (Bažant & Cedolin, 1991; ESDEP, 2018; S. P. Timoshenko & Gere, 1963).

Nowadays, guidelines for section design or local buckling in Circular Hollow Sections (CHS) remain ambiguous. Standards typically classify sections based on D / t ratios, yet adopt different design strategies:

- AISC 360-22 (American Institute of Steel Construction, 2022) provides a design procedure leading to an effective area; which is analogous to the concept of the effective width method for slender plates, except it relies on a lower mechanical background;
- CSA S16-19 (Canadian Standards Association, 2009) relies on an effective yield stress;
- Eurocode 3 (EC3, 2005) lacks explicit recommendations for slender sections. For slender cases (Class 4 sections), EC3 recommends that it should be designed following its Part 1-6 design rules, which are meant for tanks and silos, which are totally different in geometry and proportions (also, tanks and silos remain used for resisting internal pressure, not axial compression).

The difference in concepts among these standards, especially for slender sections, highlights the complexity of the issue and emphasizes the need for further improvements.

Several authors have studied the behavior of short CHS members under axial load, reporting stub column tests as well as non-linear finite element (FE) calculations (Chan et al., 2015; Guo et al., 2016; Jiao & Zhao, 2003; Ma et al., 2016a; Research Fund for Coal and Steel, 2019; Tutuncu & O'Rourke, 2006). Of prime importance, the way of introducing imperfections within the FE model has been typically defined based on the shape of the first eigenmode, scaled by different factors depending on geometrical parameters. Lately, authors have kept relying on the first eigenmode, yet artificially modifying the thickness with the goal of obtaining uniform shapes, without dependance on the D / t ratio (Meng & Gardner, 2020a).

The objective of this paper is to make a comparison between different ways of introducing generic initial imperfections, in the aim of developing reliable FE models for further studies. In this respect, stub column test data from the literature were first collected and are summarized in Section 2, accompanied with a comparison between experimental results and code predictions from various codes. Then, the development of non-linear FE numerical models is addressed in Section 3. Next, in Section 4, a discussion on the influence of the structural response of five different ways of introducing initial imperfections is proposed, along with a study related to the selection of imperfection amplitudes. Finally, recommendations on the modelling of initial imperfections within FE models are proposed.

2. Test data on CHS in compression – Design predictions from existing codes

2.1 Test data with detailed information available in literature

An extensive literature review allowed to collect some 42 stub column tests carefully documented. All collected tests contained enough information on initial imperfections, allowing an adequate development of refined non-linear finite element models. In Table 1, key parameters of the different tests are reported. It is seen that tests cover a wide range of parameters, varying from stocky to slender section shapes, from low to high strength steels and involving different fabrication processes. A typical test arrangement for a stub column test is shown in Fig. 2.

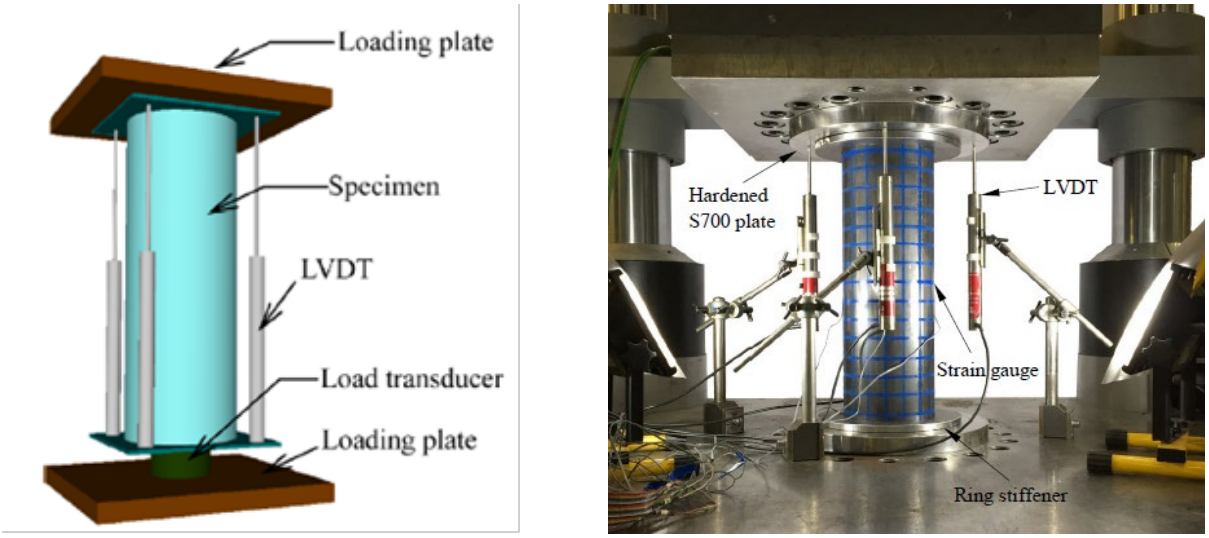

Figure 2: Test setups. (Guo et al., 2016) and (Meng & Gardner, 2020a).

It is worth mentioning that reported maximum values of initial imperfection amplitude w_0 rely on quite different experimental techniques, such as transducers or laser displacement meter, with a minimum precision of 0.01 *mm*.

Table 1: Detailed test data obtained from literature.

Test #	D [mm]	t [mm]	D / t [–]	E [MPa]	F_y [MPa]	w_0 [mm]	Fabrication	Source	Class EC3	Type AISC and CSA
1	95.5	5.3	18.0	208406	476	0.19	HR	(Chan et al., 2015)	1	Non-Slender
2	95.5	5.3	18.0	208406	476	0.23	HR	(Chan et al., 2015)	1	Non-Slender
3	95.5	5.4	17.7	208406	476	0.19	HR	(Chan et al., 2015)	1	Non-Slender
4	95.6	7.5	12.7	206374	424	0.18	HR	(Chan et al., 2015)	1	Non-Slender
5	95.6	7.4	12.9	206374	424	0.17	HR	(Chan et al., 2015)	1	Non-Slender
6	95.6	7.4	12.9	206374	424	0.07	HR	(Chan et al., 2015)	1	Non-Slender
7	150.0	2.0	75.0	188000	190	0.12	CF	(Guo et al., 2016)	2	Non-Slender
8	150.0	2.0	75.0	188000	190	0.24	CF	(Guo et al., 2016)	2	Non-Slender
9	150.0	2.0	75.0	188000	190	0.13	CF	(Guo et al., 2016)	2	Non-Slender
10	200.0	2.0	100.0	188000	190	0.59	CF	(Guo et al., 2016)	3	Non-Slender
11	200.0	2.0	100.0	188000	190	0.56	CF	(Guo et al., 2016)	3	Non-Slender
12	200.0	2.0	100.0	188000	190	0.37	CF	(Guo et al., 2016)	3	Non-Slender
13	250.0	2.0	125.0	188000	190	1.68	CF	(Guo et al., 2016)	4	Slender
14	250.0	2.0	125.0	188000	190	0.54	CF	(Guo et al., 2016)	4	Slender
15	250.0	2.0	125.0	188000	190	0.61	CF	(Guo et al., 2016)	4	Slender
16	300.0	2.0	150.0	188000	190	1.55	CF	(Guo et al., 2016)	4	Slender
17	300.0	2.0	150.0	188000	190	0.65	CF	(Guo et al., 2016)	4	Slender
18	300.0	2.0	150.0	188000	190	0.37	CF	(Guo et al., 2016)	4	Slender
19	400.0	2.0	200.0	188000	190	2.21	CF	(Guo et al., 2016)	4	Slender
20	400.0	2.0	200.0	188000	190	2.30	CF	(Guo et al., 2016)	4	Slender
21	600.0	2.0	300.0	188000	190	3.12	CF	(Guo et al., 2016)	4	Slender
22	600.0	2.0	300.0	188000	190	4.17	CF	(Guo et al., 2016)	4	Slender
23	89.0	3.9	22.8	205000	1180	0.07	CF	(Ma et al., 2016b)	4	Slender
24	139.5	5.9	23.6	205000	1180	0.17	CF	(Ma et al., 2016b)	4	Slender
25	89.0	3.0	30.1	210000	1053	0.17	CF	(Ma et al., 2016b)	4	Slender
26	140.1	4.0	35.2	213300	742	0.10	CF	(Research Fund for Coal and Steel, 2019)	4	Slender
27	140.4	4.9	28.6	212500	730	0.08	CF	(Research Fund for Coal and Steel, 2019)	3	Non-Slender
28	139.8	6.0	23.1	207900	779	0.15	CF	(Research Fund for Coal and Steel, 2019)	3	Non-Slender
29	140.1	7.9	17.8	205700	785	0.12	CF	(Research Fund for Coal and Steel, 2019)	2	Non-Slender
30	140.3	9.9	14.1	205600	788	0.10	CF	(Research Fund for Coal and Steel, 2019)	1	Non-Slender
31	168.4	4.0	42.6	211700	720	0.12	CF	(Research Fund for Coal and Steel, 2019)	4	Slender
32	193.7	5.6	34.6	217050	378	0.75	HR	(Research Fund for Coal and Steel, 2019)	2	Non-Slender
33	193.7	9.1	21.3	224000	807	1.09	CF	(Research Fund for Coal and Steel, 2019)	3	Non-Slender
34	219.1	7.0	31.3	212607	425	0.39	HR	(Research Fund for Coal and Steel, 2019)	2	Non-Slender
35	219.1	10.8	20.3	196245	942	0.42	CF	(Research Fund for Coal and Steel, 2019)	3	Non-Slender
36	219.1	10.8	20.3	196245	942	0.30	CF	(Research Fund for Coal and Steel, 2019)	3	Non-Slender
37	219.1	10.8	20.3	196245	942	0.41	CF	(Research Fund for Coal and Steel, 2019)	3	Non-Slender
38	244.0	7.5	32.5	193398	407	0.95	HR	(Research Fund for Coal and Steel, 2019)	2	Non-Slender
39	323.9	4.6	70.4	194906	429	0.61	CF	(Research Fund for Coal and Steel, 2019)	4	Slender
40	323.9	6.2	52.2	193307	372	0.92	CF	(Research Fund for Coal and Steel, 2019)	3	Non-Slender
41	323.9	8.0	40.7	200000	515	0.34	CF	(Research Fund for Coal and Steel, 2019)	3	Non-Slender
42	355.6	8.0	44.5	200000	405	0.82	HR	(Research Fund for Coal and Steel, 2019)	3	Non-Slender

2.2 Correspondence with design code predictions

Typically, current codes predict the local axial resistance of CHS depending on their D / t ratio. EC3 classifies the cross section into four different classes, while AISC 360-22 and CSA S16-19 classifies sections into slender/non-slender categories. In Fig. 3 and Table 2, results comparing code predictions to test results are summarized.

Table 2: Design predictions from codes.

	EC3*	AISC 360-22	CSA S16-19
Mean	0.92	0.97	0.89
COV	14.0%	19.3%	16.3%
% > 1.00	27%	33%	26%

*EC3 does not give straightforward rules for Class 4 sections under axial compression.

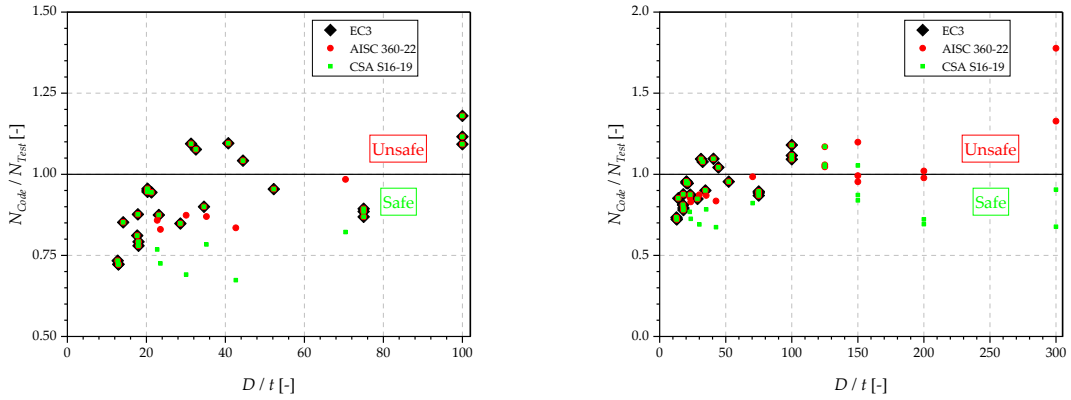

(a) Zoom on results, up to $D / t = 100$. (b) Full set of results, up to $D / t = 300$.

Figure 3: Design predictions from codes.

The major trend observed is that for the range of semi-compact to slender sections ($D / t > 80$, corresponding to Class 3 and Class 4 sections), design codes are predicting unsafe resistances – only CSA seems to provide a better approach for very high slender sections. It is also bothersome that EC3 does not give straightforward rules for the design of Class 4 sections. Accordingly, improvements in design recommendations are necessary.

3. Development of F.E. models

In order to propose improved recommendations for FE modelling in Geometrically and Materially Nonlinear Analyses with Imperfections (GMNIA) for CHS, it is first necessary to develop suitable FE models. The models were developed in the commercial FE software ABAQUS (Dassault Systemes, 2022), and rely on GMNIA analyses based on the "Riks method" as solver, allowing to handle complex and non-linear problems. The use of the S4R shell element was also adopted owing to its proven effectiveness in similar CHS studies, as cited in previous research ((Buchanan et al., 2018), (Meng et al., 2020)); this quadrangular shell element is based on Kirchhoff's bending assumptions and features reduced integration, ensuring precision in simulating the structural behavior.

Rigid body boundary conditions corresponding to thick end plates were adopted in the numerical models. Consequently, longitudinal displacement U_x of one end was prevented while on the opposite end a compression load was applied at a reference point (see Fig. 4).

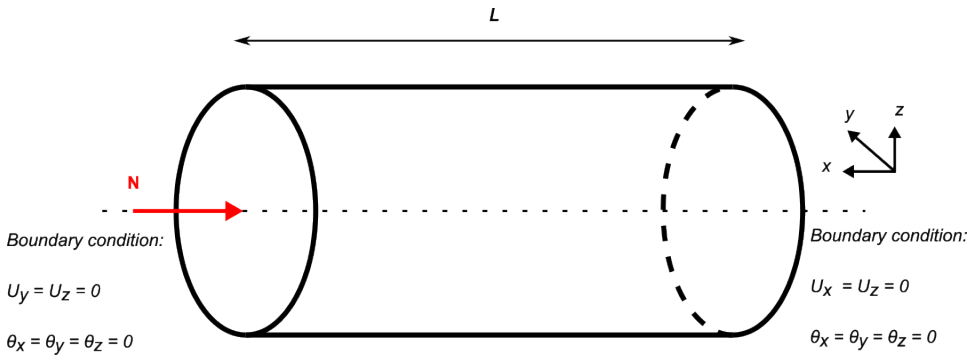

Figure 4: Boundary conditions in numerical models.

Data on dimensions, strain-stress relationships and geometric imperfections were introduced into the FE simulations following the detailed experimental measurements reported by the authors in their tests. For residual stresses, authors have indicated that they are negligible for hot-rolled sections, whereas for cold-formed sections, they are present inherently in the material stress-strain relationship (Jiao & Zhao, 2003; Research Fund for Coal and Steel, 2019; Zheng et al., 2016). Effects of residual stresses appear to become significant – around 15% difference – only for large D / t ratios (e.g., $D / t > 500$, Guo et al., 2016)); since such high slenderness ratios lie outside of the scope of CHS applications, residual stresses were not considered in this study.

It has been shown by various authors that numerical results involving shell-types responses, as is the case here, are strongly influenced by the adopted mesh density. Accordingly, a relative mesh size of $0.1 \cdot \sqrt{D.t}$ was employed for modeling the CHS stub columns. This mesh was shown to be fine enough to capture the local buckling behavior of CHS while still maintain good computational efficiency (Meng & Gardner, 2020a).

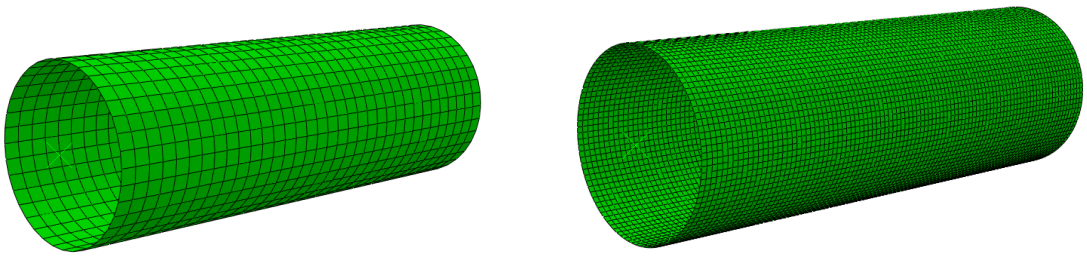

Figure 5: (a) Coarse mesh. (b) (Very) dense mesh used.

4. Sensitivity of F.E. models to initial geometrical imperfections and modeling recommendations

4.1 General considerations

Although imperfections are obviously distributed in an arbitrary way in any member, with random amplitudes, there is a need to provide general recommendations about this since all specimens cannot be measured. Normally, it is common to use the first eigenmode as the shape for initial imperfections (Ma et al., 2016b; Silvestre & Gardner, 2011; Yun et al., 2020). Beyond requiring a preliminary LBA calculation providing the buckling shape, a major inconvenience in this

procedure lies in that it makes the pattern dependent on the applied load, while real life imperfections are expressed in a somewhat random way, which cannot not load dependent. Also, in some cases this may not the best or safest choice as some authors explain (Degee et al., 2008; Farzanian et al., 2023; Pavlovčič et al., 2007; Schafer & Peköz, 1998).
Lately, different authors have presented studies based on the use of the first eigenmode, but using a modified thickness in the LBA preliminary calculation step (e.g., $t_{mod} = D / 5$), in order to "force" similar eigenshapes in all cases, without dependance on the D / t ratio (Meng et al., 2020; Meng & Gardner, 2020b; Research Fund for Coal and Steel, 2019). This procedure led to a good agreement between tests and numerical results for compact and semi-compact sections. Another classical alternative consists in defining an initially-imperfect predefined geometry, generally based on sinusoidal patterns – background of such sine-based patterns lies in elastic stability theory (Bažant & Cedolin, 1991; Den Hartog, 1952; S. P. Timoshenko & Gere, 1963).
As literature evidences, the definition of the maximum amplitude to be set plays a role as important as the shape pattern. In this way, different recommendations have been proposed (American Institute of Steel Construction, 2022; EC3, 2005; McCann et al., 2016; Meng & Gardner, 2020b), usually depending on the geometry of the sections, although a wide scatter in the measured amplitudes and proposed formulas has been reported (Meng & Gardner, 2020b).
Alternative ways to set initial geometrical imperfections are presented in the following. First, different techniques and their associated results on the influence of the shape of initial imperfections are discussed, using the measured values on amplitudes; then further examination over the effect of the amplitude is detailed.

4.2 Use of eigenmodes

At first, the initial shape investigated herein is the first eigenmode. This has been proved to be suitable for many cases, namely plate-like behavior. The popularity of this procedure comes from its simplicity, as (i) it is based on a perfect geometry, (ii) is usually readily available in commercial FE software and (iii) its application is easy to implement in extensive parametric analyses. The shape of this imperfection is shown in Fig. 6; for comparison purposes, this shape will be denoted as "Shape 1" in the following.

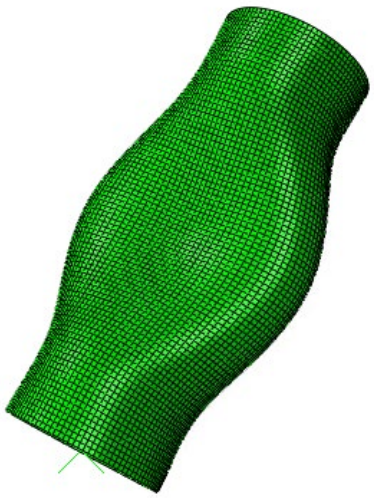

Figure 6: Shape 1 – First eigenmode.

As explained before, a variation in this "classical" approach consists in the use of the first eigenmode yet with a modified thickness $t_{mod} = D / 5$. This shape is called herein "Shape 2" and is represented in Fig. 7.

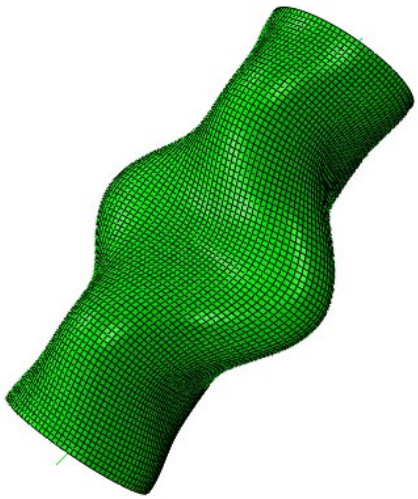

Figure 7: Shape 2 – First eigenmode for modified thickness ($t_{mod} = D / 5$).

4.3 Iterations based on post-buckling shape

The second approach is a somewhat peculiar and original procedure, which consists in an iterative scheme on the post-buckling shape (last converged step after obtaining peak load) from a prior GMNIA case with initial imperfections based on the first eigenmode (Boissonnade et al., 2006). The concept of this procedure is to provide the final post-buckling shape as initial imperfection, in the aim of including an imperfection pattern associated with the lowest resistance. However, the question that arises is if the procedure is suitable or not for parametric studies, as the computing time increases significantly through the multiple GMNIA calculation. The shape of this imperfection is shown in Fig 8 – and called Shape 3, and it is noted that it is quite different from the one of the first eigenmode (see Fig. 6). In this case, the initial geometrical imperfection shape is typically related to the "elephant foot failure" (cf. Test #1). Nevertheless, this shape may change depending on the slenderness of the section.

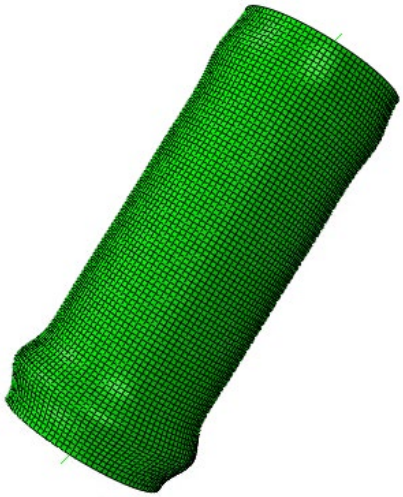

Figure 8: Shape 3 – Iterations on post-buckling shape.

4.4 Use of an annealed mode with sine waves

Another attempted way was looking for a so-called "annealed mode" within the first eigenmodes (see Fig. 9), called Shape 4. This idea came from theoretical solutions (Bažant & Cedolin, 1991; Den Hartog, 1952; S. P. Timoshenko & Gere, 1963; Ziemian, 2010) as well as from experimental observations, since the failure mode is usually defined affine to this type of pattern. In the theoretical solution, the half-wavelength associated with the critical load is given by Eq. (1).

$$\lambda_0 = 1.73\sqrt{r \cdot t} \tag{1}$$

Aa per eigenmodes, this shape remains the closest to a so-called "elephant foot failure mode", which is described in many experimental reports and papers (Batikha et al., 2009; Bock et al., 2023; Saha & Matsagar, 2015). Corresponding practical implementation remains fastidious since the corresponding buckling mode usually is not the first one, and has to be found within the list of the first eigenmodes, making this procedure unsuited for extensive parametric studies.

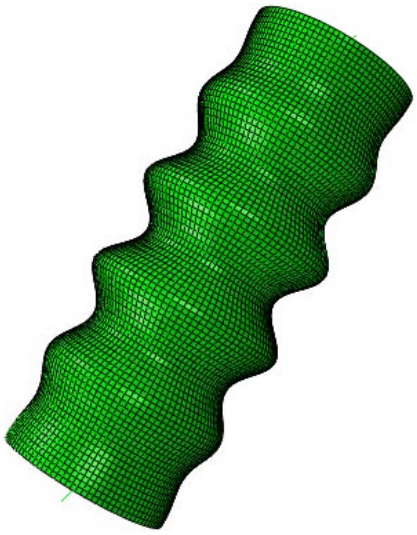

Figure 9: Shape 4 – Annealed mode pattern.

To overcome this issue, a last shape was studied by using an imperfect geometry defined through a sinusoidal pattern. Different half-wavelengths were employed, and a correlation was observed: as the half-wavelength became smaller (i.e., the number of half-waves increased), FE ultimate loads decreased as well, as shown in Fig. 10.

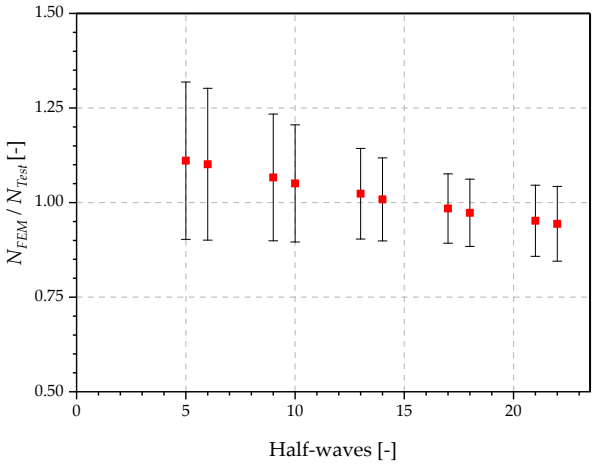

Figure 10: Number of half waves influence.

Based on these observations, a recommendation on the half-wavelength to adopt could be established, as is proposed in Eq. (2).

$$\lambda_0 = \frac{D^{0.35} \cdot t^{0.65} \cdot E}{170 \cdot F_y} \tag{2}$$

A comparison between different number of half-waves, the results of the theorical formula (Eq. (1)) and the proposed Eq. (2) are presented in Table 3. The proposed Eq. (2) provides adequate results as an average value of 1.00 is observed in Table 3, along with a quite low COV of 7.6%; this definition shall be used as the half-wavelength for the sinusoidal imperfection pattern, called Shape 5, shown in Fig. 11.

Table 3: Half-wavelength influence.

	5 Half-waves	10 Half-waves	22 Half-waves	Eq. (1)	Eq. (2)
Mean	1.11	1.05	0.94	0.89	1.00
COV	18.7%	14.7%	10.5%	18.6%	7.6%
Min.	0.97	0.93	0.65	0.44	0.81
Max.	2.16	1.84	1.10	1.07	1.19
% < 0.90	0.0%	0.0%	21.4%	33.3%	7.1%
% > 1.10	33.3%	11.9%	0.0%	0.0%	7.1%

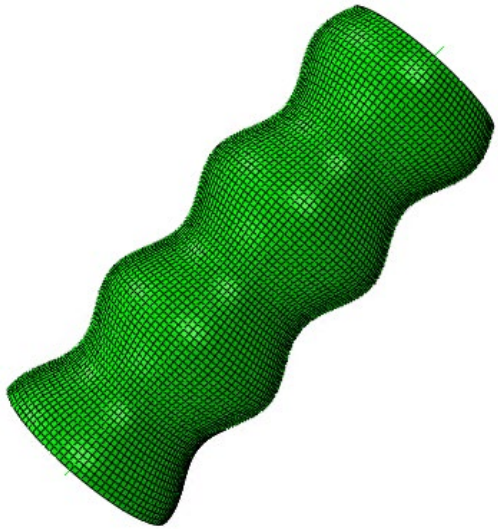

Figure 11: Shape 5 – Sinusoidal pattern (Test #1 – λ_0 = 73 *mm* – 6.5 half-waves).

Is important to remark that for this type of imperfection pattern, the mesh shall be fine enough to allow multiple elements to be in each half-wave. The recommendations from (Meng & Gardner, 2020a), proved to be sufficient in this respect.

4.5 Results on initial imperfections shapes

So far, five different geometrical imperfection patterns were presented (Shape 1: first eigenmode, Shape 2: first eigenmode with modified thickness for the LBA computation, Shape 3: iterations on post-buckling shape, Shape 4: annealed eigenshape, and Shape 5: sinusoidal pattern). In Table 4, a comparison between the numerical FE results obtained with these assumptions and the experimental tests is reported – note that for each FE simulation, measured amplitudes of the imperfections were considered.

Table 4: Comparison between N_{FEM} / N_{TEST} for different shapes.

	Shape 1	Shape 2	Shape 3	Shape 4	Shape 5
Mean	1.09	1.09	1.04	0.98	1.00
COV	15.2%	14.9%	9.9%	6.8%	7.6%
Min.	0.97	0.97	0.93	0.82	0.81
Max.	1.91	1.88	1.50	1.09	1.19
% < 0.90	0.0%	0.0%	0.0%	11.9%	7.1%
% > 1.10	28.6%	28.6%	16.7%	0.0%	7.1%

It can be seen in Table 4 that for the first two shapes, which are based on the first eigenmode, a high COV (15%) is obtained, as well as an important percentage of unsafe values (around 28%) and a high maximum value (approx. 1.90), compared to the last two shapes which are based on an annealed pattern. The observed behavior for Shape 3 is not good enough to support the computational expense that it requires. Although the two last shapes obtained a good agreement, the Shape 4 approach is deemed not suitable for extensive studies as the eigenmode number needs to be sought in any case; eventually, Shape 5 happens to be the best option according to (i) the good quality of the obtained results and to (ii) its possibility to be systematically implemented (no need to run previous analyses or to search for particular eigenmode).

Nevertheless, the observed odd behavior for the first two shapes can be shown in large parts to be associated to (very) slender sections. In Table 5, the same results are presented, excluding the tests with D / t ratios greater than or equal to 100.

Table 5: Comparison between N_{FEM} / N_{TEST} for different shapes (D / t < 100).

	Shape 1	Shape 2	Shape 3	Shape 4	Shape 5
Mean	1.03	1.02	1.00	0.98	0.99
COV	4.5%	4.6%	5.0%	5.7%	5.1%
Min.	0.97	0.97	0.93	0.87	0.88
Max.	1.10	1.10	1.09	1.08	1.08
% < 0.90	0.0%	0.0%	0.0%	6.9%	3.4%
% > 1.10	3.4%	3.4%	0.0%	0.0%	0.0%

It is noted that for non-slender sections, all shapes happen to have a good agreement with the experimental tests. It is then concluded that a special treatment shall be foreseen for the most slender cases.

4.6 Amplitude of initial imperfections

To this point, all the discussion remained centered over the pattern of initial imperfections, but the amplitude w_0 has not been examined so far. Different codes and authors have proposed expressions for the calculation of the maximum amplitude: (Meng & Gardner, 2020a) proposed Eq. (3), while Eq. (4) recalls the recommendations of EC3 and AISC. The parameter Q for AISC shall be taken equal to 16.5 while in EC3 Q = 16, 25 or 40, depending on the quality of the manufacturing. Another typical way of defining w_0 consists in using 1% of the thickness, as is presented in Eq. (5).

$$w_0 = 0.01\sqrt{r \cdot t} \tag{3}$$

$$w_0 = \frac{1}{Q}\sqrt{\frac{r}{t}} \cdot t \tag{4}$$

$$w_0 = 0.01 \cdot t \tag{5}$$

FE results obtained with amplitudes set from each proposal and based on Shape 5 are plotted in Fig. 12 and compared to the reported values of maximum amplitude (max. measured amplitudes). It is seen that for non-slender sections (D / t < 80), the proposed equations return values that are significantly greater than the measured amplitudes, while for slender sections, the equations seem to underestimate the maximum amplitude.

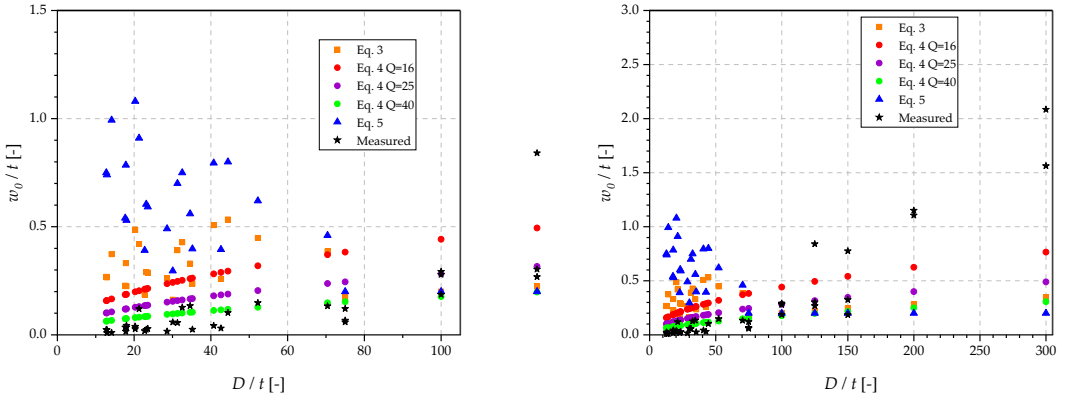

(a) Zoom on results, up to $D / t = 100$. (b) Full set of results, up to $D / t = 300$.

Figure 12: Amplitude of initial imperfections.

Therefore, to remedy this, Eq. (6) is proposed. Fig. 13 shows that the behavior of the proposed equation is more consistent with the reported values, whatever the slenderness range. Also, Eq. (6) proposal provides safe yet realistic w_0 values. In Table 6, statistical results on the various equations considered for w_0 are presented; Eq. (6) is shown to achieve the best results, namely leading to the lowest (i) COV and (ii) number of unsafe results.

$$w_0 = \frac{1}{2000}\left(\frac{D}{t}\right)^{1.5} \tag{6}$$

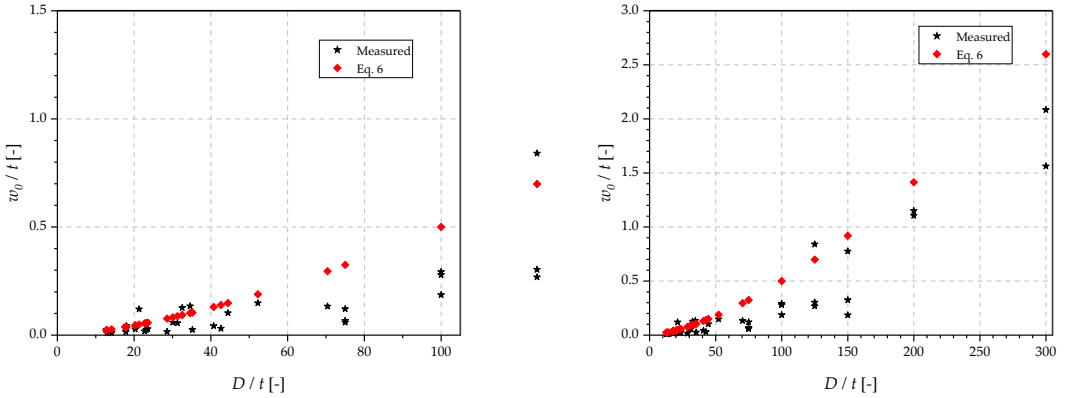

(a) Zoom on results, up to $D / t = 100$. (b) Full set of results, up to $D / t = 300$.

Figure 13: Proposed equation on amplitude of initial imperfections.

Table 6: N_{FEM} / N_{TEST} for different amplitudes.

	Measured	Eq. (3)	Eq. (4) $Q = 16$	Eq. (4) $Q = 25$	Eq. (4) $Q = 40$	Eq. (4) $Q = 16.5$	Eq. (5)	Eq. (6)
Mean	1.00	1.07	0.92	0.99	1.03	0.93	1.05	0.95
COV	7.6%	19.1%	19.1%	18.8%	18.9%	19.1%	21.8%	9.3%
Min.	0.81	0.90	0.69	0.78	0.85	0.69	0.86	0.75
Max.	1.19	2.09	1.69	1.87	1.99	1.70	2.15	1.12
% < 0.90	7.1%	2%	50%	36%	14%	50%	29%	21%
% > 1.10	7.1%	24%	12%	17%	19%	12%	26%	2%

In Table 7, the same statistical analysis is done for non-slender sections ($D / t < 100$). In this case, Eq. (3), Eq. (4) with $Q = 40$, Eq. (5) and Eq. (6) all provide adequate results.

Table 7: N_{FEM} / N_{TEST} for different amplitudes ($D / t < 100$).

	Measured	Eq. (3)	Eq. (4) $Q = 16$	Eq. (4) $Q = 25$	Eq. (4) $Q = 40$	Eq. (4) $Q = 16.5$	Eq. (5)	Eq. (6)
Mean	0.99	0.98	0.84	0.91	0.95	0.85	0.94	0.96
COV	5.1%	5.2%	10.2%	7.5%	6.0%	10.0%	6.3%	6.8%
Min.	0.88	0.90	0.69	0.78	0.85	0.69	0.86	0.82
Max.	1.08	1.07	0.98	1.02	1.05	0.98	1.05	1.08
% < 0.90	3.4%	3%	72%	52%	21%	72%	41%	14%
% > 1.10	0.0%	0%	0%	0%	0%	0%	0%	0%

Given its applicability to both slender and non-slender cases, it is advisable to use Eq. (6) for describing the maximum imperfection amplitude when resorting to the proposed sinusoidal imperfection pattern (Shape 5).

4.7 Modelling recommendations

Based on the previous results, it is then recommended to use a sinusoidal imperfection pattern, as presented in Section 4.4, with the wavelength proposed in Eq. (2) and with an amplitude ruled by Eq. (6). This proved adequate for all ranges of slenderness, contrary to imperfections patterns based on the first eigenmode who showed inaccurate for slender sections.

5. Conclusions

This paper presented a study on the stability behavior of CHS shapes under compression; more precisely, the paper focused on the sensitivity to initial imperfections, using detailed test results available in the literature. Then, for these test results, GMNIA FE numerical models were developed, validated and used for a sensitivity analysis on initial imperfections. A comparison between different ways to introduce the distribution and amplitude of initial imperfections was also described, and the main observations can be summarized as follows:

1. A proposal to introduce initial imperfections, based on a sinusoidal shape aiming to be on the safe side for slender sections was presented;
2. There is a limited number of experimental tests on slender CHS sections. This led to extrapolation of the results and behavior from compact shapes, while their behavior is quite different. Slender sections of course showed very sensitive to initial imperfections, compared to compact shapes;

3. The current way of introducing initial imperfections, using the shape of the first eigenmode with a modified thickness, along with the equations to estimate the amplitude of the initial imperfection was found adequate for compact sections yet unsafe for large D / t ratios (slender sections);
4. Current codes have limited information on the design of slender sections. CSA S16-19 and AISC 360-22 seem to provide unsafe predictions compared to tests, being more critical in the case of the AISC code, while EC3 does not have clear rules for design of slender CHS columns, using the design approach for tanks and silos. Further experimental studies need to be undertaken to improve the design rules for these types of sections.

References

American Institute of Steel Construction. (2022). *Specification for Structural Steel Buildings*.

Batikha, M., Chen, J. F., Rotter, J. M., & Teng, J. G. (2009). Strengthening metallic cylindrical shells against elephant's foot buckling with FRP. *Thin-Walled Structures*, *47*(10), 1078–1091. https://doi.org/10.1016/j.tws.2008.10.012

Bažant, Z., & Cedolin, L. (1991). *Stability of Structures: Elastic, Inelastic, Fracture and Damage Theories*. Oxford University Press.

Bock, M., Bawazeer, J., Robinson, J., Theofanous, M., & Skalomenos, K. (2023). Structural performance of additive manufactured aluminum tubular stub columns. *Ce/Papers*, *6*(3–4), 751–756. https://doi.org/10.1002/cepa.2603

Boissonnade, N., Degée, H., Naumes, J., & Oppe, M. (2006). Experimental and numerical investigations for I-girders in bending and shear stiffened by closed trapezoidal stiffeners. *ICMS*.

Buchanan, C., Real, E., & Gardner, L. (2018). Testing, simulation and design of cold-formed stainless steel CHS columns. *Thin-Walled Structures*, *130*, 297–312. https://doi.org/10.1016/j.tws.2018.05.006

Canadian Standards Association. (2009). *CSA S16-09—Design of steel*.

Chan, T.-M., Huai, Y.-M., & Wang, W. (2015). Experimental investigation on lightweight concrete-filled cold-formed elliptical hollow section stub columns. *Journal of Constructional Steel Research*, *115*, 434–444. https://doi.org/10.1016/j.jcsr.2015.08.029

Dassault Systemes. (2022). *Abaqus 2022* [Computer software].

Degee, H., Boissonnade, N., & Maquoi, R. (2008). Numerical investigations on web panels stiffened by one or two trapezoidal stiffeners. *Fifth International Conference on Coupled Instabilities in Metal Structures*.

Den Hartog, J. P. (1952). *Advanced strength of materials*. McGraw Hill.

EC3. (2005). *EN 1993-1-1: Eurocode 3—Design of steel structures—Part 1-1: General rules and rules for buildings*. European Committee for Standardization (CEN).

ESDEP. (2018). *Lectures on Structural Steel*.

Farzanian, S., Louhghalam, A., Schafer, B. W., & Tootkaboni, M. (2023). Geometric imperfections in CFS structural members: Part I: A review of the basics and some modeling strategies. *Thin-Walled Structures*, *186*, 110619. https://doi.org/10.1016/j.tws.2023.110619

Guo, L., Liu, Y., Jiao, H., & An, S. (2016). Behavior of thin-walled circular hollow section stub columns under axial compression. *International Journal of Steel Structures*, *16*(3), 777–787. https://doi.org/10.1007/s13296-015-0159-0

Jiao, H., & Zhao, X.-L. (2003). Imperfection, residual stress and yield slenderness limit of very high strength (VHS) circular steel tubes. *Journal of Constructional Steel Research*, *59*(2), 233–249. https://doi.org/10.1016/S0143-974X(02)00025-1

Ma, J.-L., Chan, T.-M., & Young, B. (2016a). Experimental Investigation on Stub-Column Behavior of Cold-Formed High-Strength Steel Tubular Sections. *Journal of Structural Engineering*, *142*(5), 04015174. https://doi.org/10.1061/(ASCE)ST.1943-541X.0001456

Ma, J.-L., Chan, T.-M., & Young, B. (2016b). Experimental Investigation on Stub-Column Behavior of Cold-Formed High-Strength Steel Tubular Sections. *Journal of Structural Engineering*, *142*(5), 04015174. https://doi.org/10.1061/(ASCE)ST.1943-541X.0001456

McCann, F., Fang, C., Gardner, L., & Silvestre, N. (2016). Local buckling and ultimate strength of slender elliptical hollow sections in compression. *Engineering Structures*, *111*, 104–118. https://doi.org/10.1016/j.engstruct.2015.12.020

Meng, X., & Gardner, L. (2020a). Cross-sectional behaviour of cold-formed high strength steel circular hollow sections. *Thin-Walled Structures*, *156*, 106822. https://doi.org/10.1016/j.tws.2020.106822

Meng, X., & Gardner, L. (2020b). Simulation and design of semi-compact elliptical hollow sections. *Engineering Structures*, *202*, 109807. https://doi.org/10.1016/j.engstruct.2019.109807
Meng, X., Gardner, L., Sadowski, A. J., & Rotter, J. M. (2020). Elasto-plastic behaviour and design of semi-compact circular hollow sections. *Thin-Walled Structures*, *148*, 106486. https://doi.org/10/ghdwh8
Pavlovčič, L., Detzel, A., Kuhlmann, U., & Beg, D. (2007). Shear resistance of longitudinally stiffened panels—Part 1: Tests and numerical analysis of imperfections. *Journal of Constructional Steel Research*, *63*(3), 337–350. https://doi.org/10.1016/j.jcsr.2006.05.008
Petersen, C. (2012). *Stahlbau: Grundlagen der Berechnung und baulichen Ausbildung von Stahlbauten*. Springer-Verlag.
Petersen, C. (2020). *Statik und Stabilität der Baukonstruktionen: Elasto-und plasto-statische Berechnungsverfahren druckbeanspruchter Tragwerke: Nachweisformen gegen Knicken, Kippen, Beulen*. Springer-Verlag.
Research Fund for Coal and Steel. (2019). *Overall-Slenderness Based Direct Design for Strength and Stability of Innovative Hollow Sections. HOLLOSSTAB* (RFCS-2015-709892).
Rotter, J. M. (2023). *Structural and Functional Design of Metal Silos*. CRC Press.
Saha, S. K., & Matsagar, V. A. (2015). Reliability of Base-Isolated Liquid Storage Tanks under Horizontal Base Excitation. In S. Kadry & A. El Hami (Eds.), *Numerical Methods for Reliability and Safety Assessment* (pp. 305–328). Springer International Publishing. https://doi.org/10.1007/978-3-319-07167-1_10
Schafer, B. W., & Peköz, T. (1998). Computational modeling of cold-formed steel: Characterizing geometric imperfections and residual stresses. *Journal of Constructional Steel Research*, *47*(3), 193–210. https://doi.org/10.1016/S0143-974X(98)00007-8
Silvestre, N., & Gardner, L. (2011). Elastic local post-buckling of elliptical tubes. *Journal of Constructional Steel Research*, *67*(3), 281–292. https://doi.org/10.1016/j.jcsr.2010.11.004
Timoshenko, S. (1959). *Theory of Plates and Shells.* McGraw Hill.
Timoshenko, S. P., & Gere, J. M. (1963). *Theory of Elastic Stability* (2nd ed.). Mc Graw Hill International Book Company.
Tutuncu, I., & O'Rourke, T. D. (2006). Compression Behavior of Nonslender Cylindrical Steel Members with Small and Large-Scale Geometric Imperfections. *Journal of Structural Engineering*, *132*(8), 1234–1241. https://doi.org/10.1061/(ASCE)0733-9445(2006)132:8(1234)
Yun, X., Wang, Z., & Gardner, L. (2020). Structural performance and design of hot-rolled steel SHS and RHS under combined axial compression and bending. *Structures*, *27*, 1289–1298. https://doi.org/10.1016/j.istruc.2020.06.038
Zheng, B., Shu, G., Xin, L., Yang, R., & Jiang, Q. (2016). Study on the Bending Capacity of Cold-formed Stainless Steel Hollow Sections. *Structures*, *8*, 63–74. https://doi.org/10.1016/j.istruc.2016.08.007
Ziemian, R. D. (2010). *Guide to stability design criteria for metal structures*. John Wiley & Sons.